

Supplementary Information for

Tuning the oscillatory dynamics of Belousov-Zhabotinsky reaction using ruthenium nanoparticles decorated graphene

D. Jaya Prasanna Kumar, Sachin Verma, Kabeer Jasuja, Pratyush Dayal*

Department of Chemical Engineering, Indian Institute of Technology Gandhinagar, Gandhinagar, Gujarat 382355, India

*pdayal@iitgn.ac.in

The BZ oscillating reaction

The Belousov-Zhabotinsky (BZ) reaction is a widely studied oscillating reaction, in which an organic substrate is oxidized in the presence of a metal ion catalyst under acidic conditions.¹⁻³ The mechanism of BZ reaction is quite complex with 80 elementary steps, and 26 variable chemical species concentration.⁴ Field *et al.* proposed a simplified model for BZ reaction at the University of Oregon, which is known as the Oregonator model.² The mechanism described using this model is FKN mechanism,³ which comprises a set of three competent processes as shown in Figure S1.

S1 Competent cyclic subreactions of BZ reaction

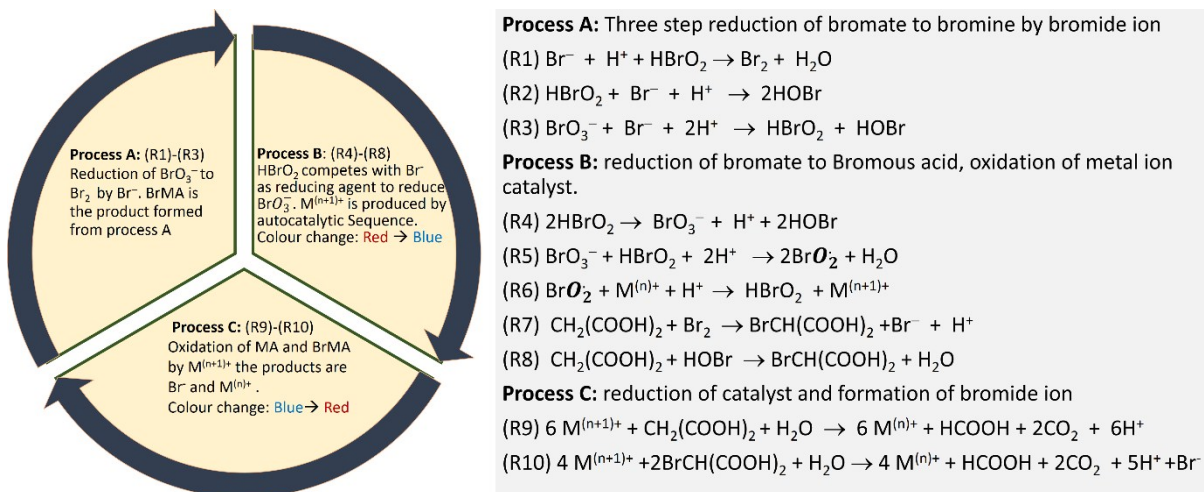


Figure S1. Left panel: Pictorial representation of three competent cyclic sub-reactions, i.e., Process A, Process B and Process C of BZ reaction. Right panel: FKN reaction mechanism for three processes. Process A: Inhibitor Br^- is consumed, process B: oxidation of metal ion catalyst, process C: formation of Br^- and reduction of metal ion catalyst thereby paving the way for process A and process B.

The reactions shown in Fig. S1 (right panel) are further summarized into five reactions that is popularly known as Oregonator scheme. These reactions and the corresponding nonlinear ordinary differential equations (ODE's) are tabulated below.²

| Rate equations of Oregonator Scheme | ODE's of the Oregonator model |
|--|---|
| $A + Y \rightarrow X + P$ Rate = k_1AY $k_1 = k_{R3}[H^+]^2$ | $\frac{dX}{dt} = k_1AY - k_2XY + k_3AX - 2k_4X^2$ $\frac{dY}{dt} = -k_1AY - k_2XY + \frac{1}{2}fk_5BZ$ $\frac{dZ}{dt} = 2k_3AX - k_5BZ$ |
| $X + Y \rightarrow 2P$ Rate = k_2AY $k_2 = k_{R2}[H^+]$ | |
| $A + X \rightarrow 2X + 2Z$ Rate = k_3AX $k_3 = k_{R5}[H^+]$ | |
| $X + X \rightarrow A + P$ Rate = k_4X^2 $k_4 = k_{R4}[H^+]$ | |
| $B + Z \rightarrow \frac{1}{2}fY$ Rate = k_5BZ | |
| Here A = $[BrO_3^-]$, B = [Organic species], X=[HBrO ₂], Y = [Br-], Z= $[M^{(n+1)+}]$, f = stoichiometric coefficient. | |

The colour of the reaction mixture continuously changes between blue and red colours, in the presence of ferroin indicator, as BZ reaction goes through three competent subreactions shown above. The cycling of red and blue colors of BZ reaction mixture is depicted pictorially in Figure S2 (a), and the corresponding graphical representation of the oxidized state of the metal ion catalyst is shown in Figure S2 (b). The three cyclic processes compete with each other and ultimately, the system attains equilibrium as the organic substrate present in the system gets exhausted.⁵

S2 Oscillations in BZ reaction manifested as colour change

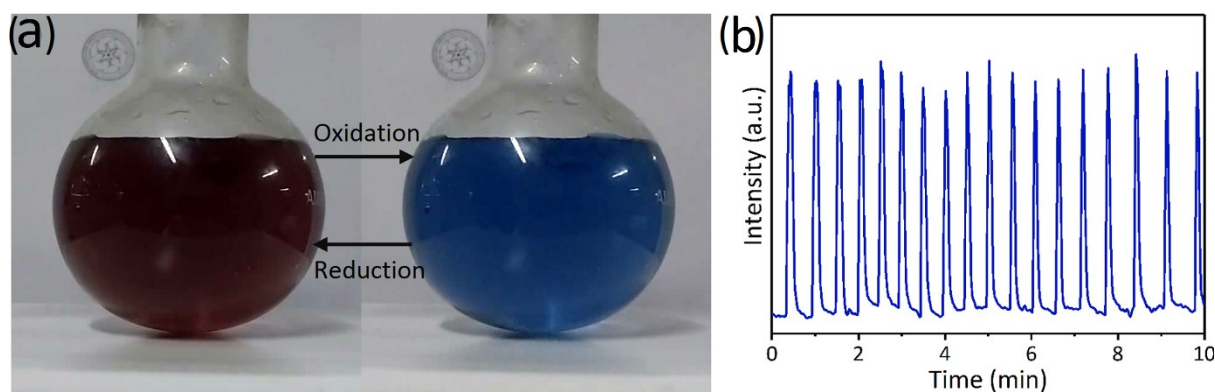


Figure S2. Left panel: BZ reaction depicting red and blue colour changes when the metal ion catalyst cycles through reduced and oxidized states in the presence of ferroin. Right panel: graphical representation of the oscillation of oxidized states of metal ion catalyst in BZ solution.

S3 Zeta Potential of graphene oxide (GO), reduced graphene oxide (rGO), and graphene

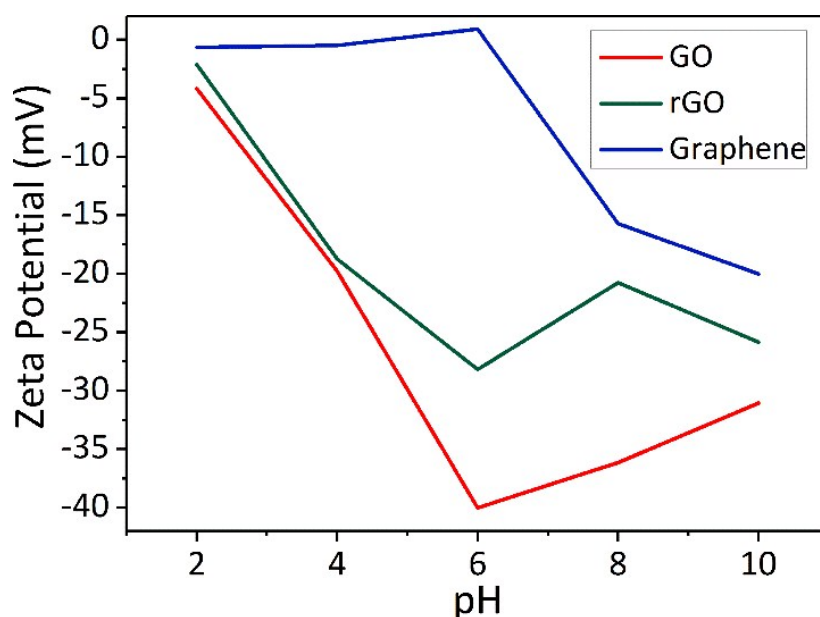


Figure S3. Zeta Potential (surface charge) of graphene oxide, reduced graphene oxide, and graphene as a function of pH in aqueous dispersion at concentration 0.05 mg/mL.

The zeta potential of the samples are analyzed with NICOMP 380 ZLS using dilute dispersions of 0.05 mg/mL of GO, rGO, and graphene. 1 ml of the sample is taken in a cuvette with platinum electrodes. The measurements are carried out by varying the pH from 2-10. A highly negative charge on GO is attributed to the presence of oxy-functional groups.⁶

S4 UV and XRD spectra of Ru-GO, Ru-rGO, Ru-graphene

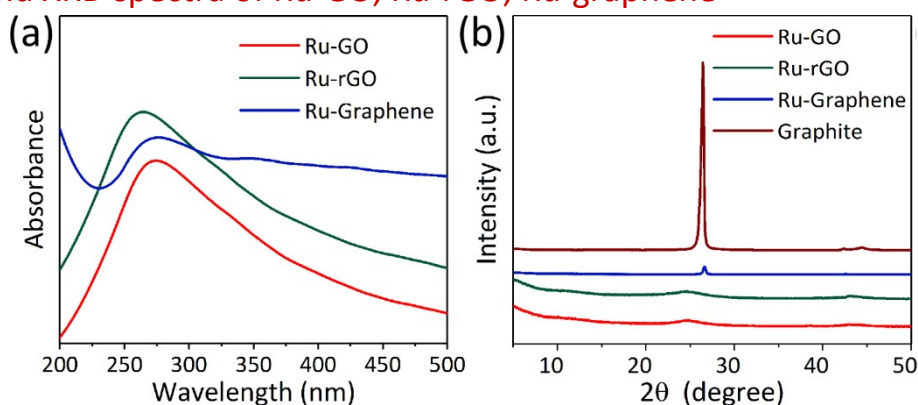


Figure S4. (a) UV-Vis spectra of Ru-GO, Ru-rGO, and Ru-Graphene, shows a peak around 270 nm indicating GO, and rGO have reduced completely. (b) XRD spectra of Ru-GO, Ru-rGO, and Ru-Graphene shows a peak around 25° indicates formation of graphene from GO and rGO.

The UV-Visible absorption spectra of the synthesized Ru-GO, Ru-rGO and Ru-graphene nanocomposite are shown in Fig. S4 (a). The absorption peak around 270 nm for all the samples suggests that ascorbic acid has reduced GO, and rGO completely and π conjugation network^{7,8} is restored. Figure S4 (b) depicts X-ray diffraction pattern (XRD) of synthesized Ru-GO, Ru-rGO and Ru-graphene

nanocomposites. All the composites have peaks around 25° , which confirm the reduction of GO and rGO to form graphene.⁷ An additional peak around 43° corresponds to disordered carbon layers commonly referred to as turbostratic disorder.⁹

S5 FESEM and TEM images of Ru-GO, Ru-rGO, Ru-graphene

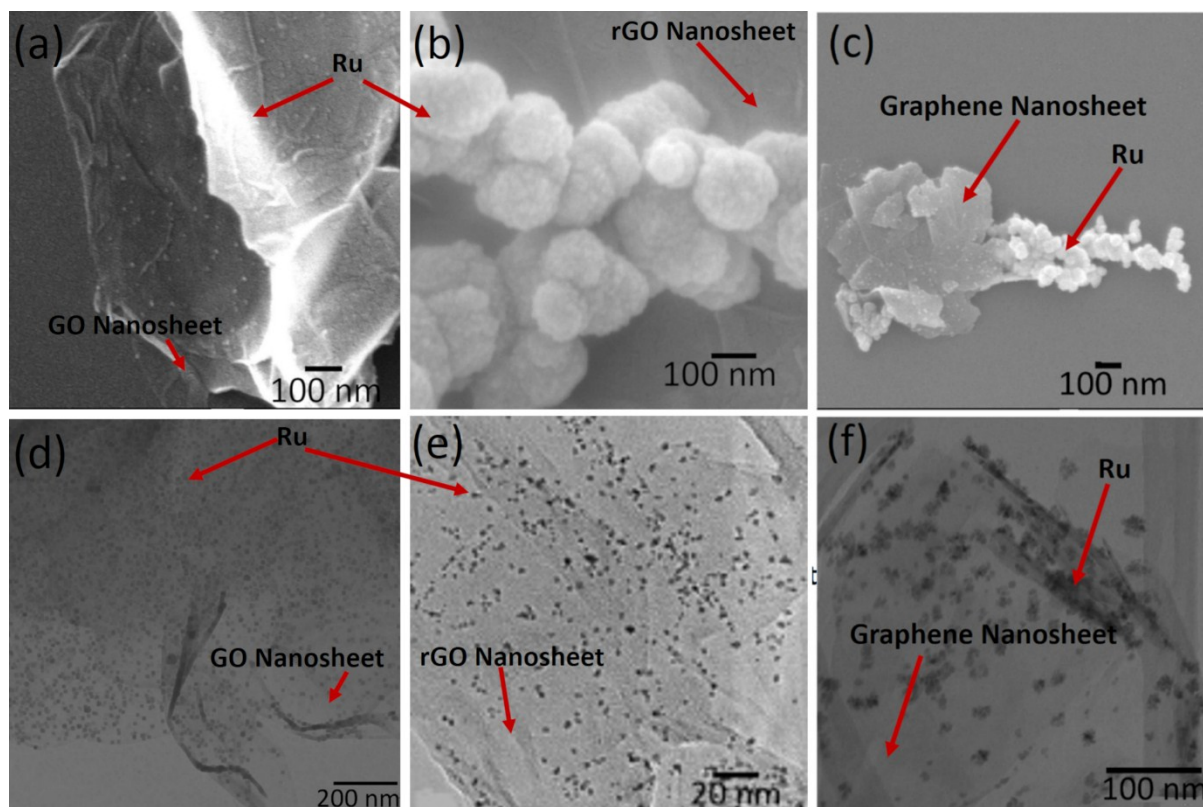


Figure S5. FESEM images of Ru-GO, Ru-rGO, and Ru-graphene shown in (a),(b), and (c), respectively show wrinkled sheet-like structures with Ru nanoparticles (marked by arrows) attached to the surface. The TEM images of Ru-GO, Ru-rGO, and Ru-graphene are shown in (d),(e), and (f), respectively show few layered nanosheets with Ru nanoparticles (dark spots) of average size between 2-3 nm, decorated to the nanosheet surface.

FESEM images shown in Fig. S5(a)-(c) reveal wrinkled sheet-like structures of size $0.5-10\ \mu\text{m}$ decorated with RuNP confirmed by EDS. TEM micrographs, shown in Figure S5(d)-(f), reveal the presence of sheet-like structures with lateral dimensions of $\sim 2\ \mu\text{m}$, with uniform decoration of Ru nanoparticles.

S6 Particle size distribution of Ru-rGO, and Ru-graphene

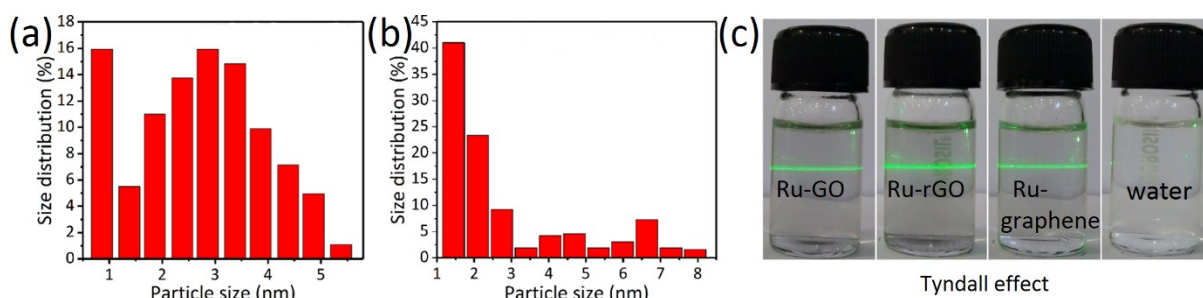


Figure S6. Particle size distribution of (a) Ru-rGO, (b) Ru-graphene (correspond to Figs. 2(e) & 2(h) of the manuscript) determined from ImageJ software using TEM image. (c) Stable colloidal dispersions of Ru-GO, Ru-rGO, and Ru-graphene compared to pure DI water.

Fig S6 (a) and (b) show the particle size distribution RuNPs of average size 2-3 nm on the synthesized nanocomposites Ru-GO and Ru-rGO, respectively; the size of the nanoparticles is measured with ImageJ software using the TEM image. Fig. S6 shows stable colloidal dispersions of various nanocomposites kept over a period of two months.

S7 XPS survey scan of Ru-GO, Ru-rGO, and Ru-graphene

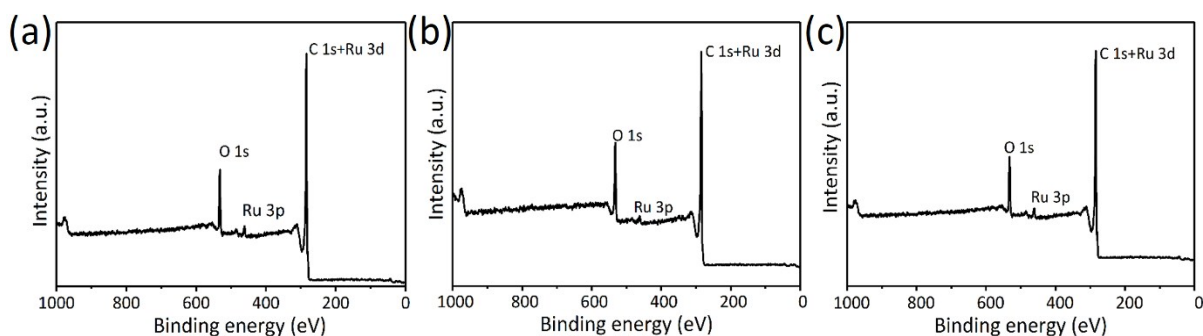


Figure S7. XPS survey peaks of (a) Ru-GO, (b) Ru-rGO, and (c) Ru-graphene. The peaks for C 1s, Ru 3d, Ru 3p, and O 1s at 285, 465 and 530 eV are observed.

X-ray photoelectron spectroscopy (XPS) analysis is carried out to determine the chemical composition of synthesized Ru-GO, Ru-rGO, and Ru-graphene nanocomposites (see Fig. S7). The Ru 3p peak at 465 eV and Ru 3d peak at 284 eV in the survey scan confirm the existence of Ruthenium.^{10,11}

S8 XPS C 1s, Ru 3p scan of Ru-rGO, and Ru-graphene

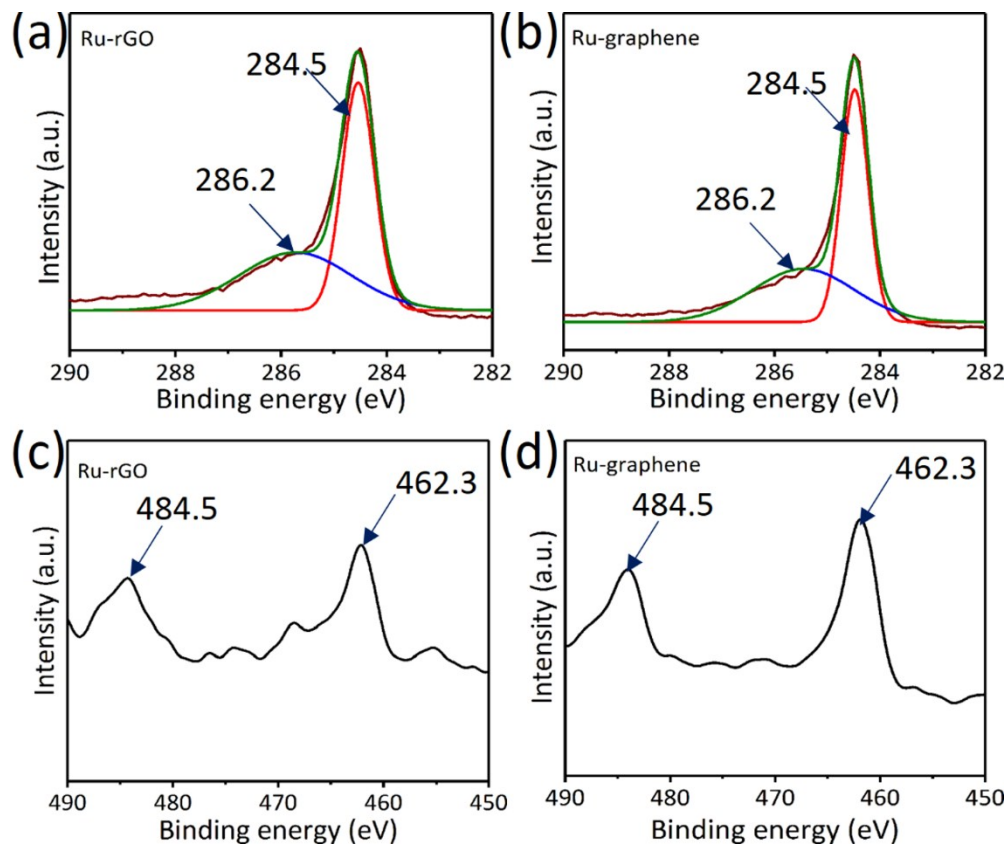


Figure S8. XPS analysis of Ru-GO and Ru-graphene. The C 1s spectra of (a) Ru-rGO and (b) Ru-graphene shows the presence of C-C/C=C (284.5 eV) and C-O (286.4 eV). The Ru 3p spectra of (c) Ru-GO and (d) Ru-graphene confirm the presence of Ru at 462.3 eV (Ru 3P_{3/2}) and 484.5 eV (Ru 3P_{1/2}).

Figure S8 (a) and (b) depicts C 1s spectra of Ru-rGO and Ru-graphene and reveals the existence of C-C/C=C (284.5 eV) and C-O (286.4 eV) thus confirming the significant removal of oxy-functional groups.⁷ The existence of elemental and oxidized ruthenium are observed around 462 eV and 485 eV, respectively for Ru-rGO (Fig. S8(c)) and Ru-graphene (Fig. S8(d)) samples.¹²

S9 Measurement of electrical conductivity of samples

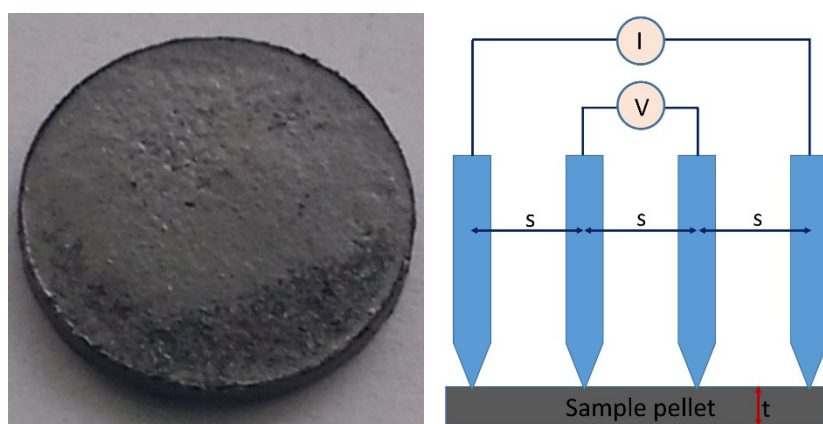


Figure S9. Left panel: Samples are made into pellets of diameter 10 mm with a 3-ton pressure, right panel: four probe resistivity measuring instrument used to measure the current for the known applied voltage.

The conductivity of the samples is determined using four-point probe resistivity measuring instrument shown in Fig. S9. Typically, the dried nanocomposite sample is made into pellets of diameter 10 mm. The resistivity ρ of the sample measured as the function of pellet thickness t , measured voltage V , and applied current I .¹³ The measured values of conductivity for Ru-GO, Ru-rGO and Ru-Graphene are 3866, 5157, and 7477 S/m, respectively.

S10 Determination of oscillation frequency of BZ reaction by image processing



Figure S10A Frames of BZ video extracted from video recording of the BZ reaction.

We used the image processing methodology to measure the frequency of chemical oscillations in the BZ reaction. The BZ reaction is carried out and its video is captured in real-time by a camera. The video is then transferred to a computer for processing where video frames are saved as an image; these images are shown in Fig. S10A. Subsequently, the intensity of blue colour from each image is extracted and plotted against time. The frequency is then calculated by counting the number of peaks in intensity obtained over a period of 10 mins.

Comparison between image processing methodology and potentiometric techniques

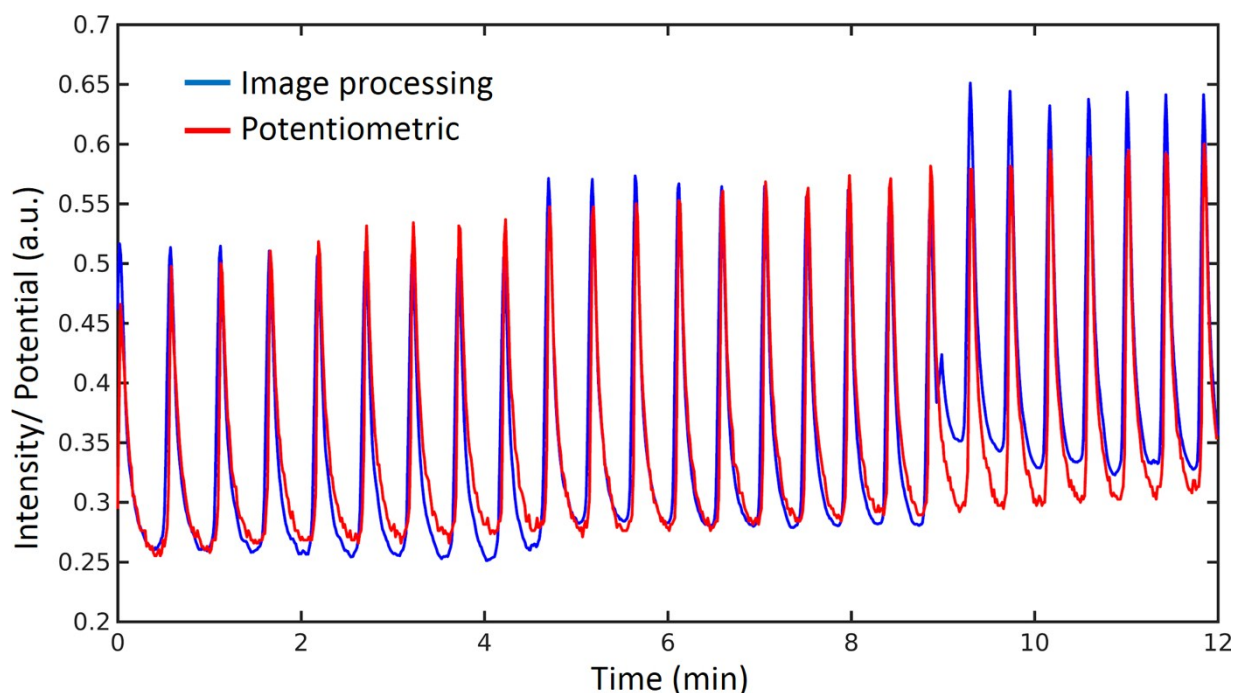


Figure S10B Comparison between image processing and potentiometric methods for the measurement of oscillating frequency of the BZ reaction catalysed by traditional solution based catalyst.

The oscillating frequency of the BZ reaction was measured with image processing methodology (IPM) which was validated with commonly used potentiometric technique. In Figure S10B, we witnessed that both the measurements, from the potentiometry and from IPM, match for the BZ system catalysed by traditional solution based catalyst. The analysis for the effect of BZ nanocatalyst, however, was carried out using IPM, and hence the color of the nanocomposite (dark grey/black) is expected to interfere with the color of the BZ reagents. In other words, the use of our BZ nanocatalyst lowers the contrast of the red and blue colors, which might not be attributed to the reduction in the amplitude, unless verified independently with another established method.

S11 Wave form of the BZ reaction with cerium, Ru-GO, Ru-rGO, and Ru-graphene

The spatiotemporal patterns (waveform) of the BZ reaction with cerium, Ru-GO, Ru-rGO, and Ru-graphene is shown in Figure S11. Due to the presence of highly conductive graphene dispersed uniformly in the BZ reagents, there are multiple nucleation centers and thus, almost the entire solution in the Petri dish switches rapidly between red and blue colors.

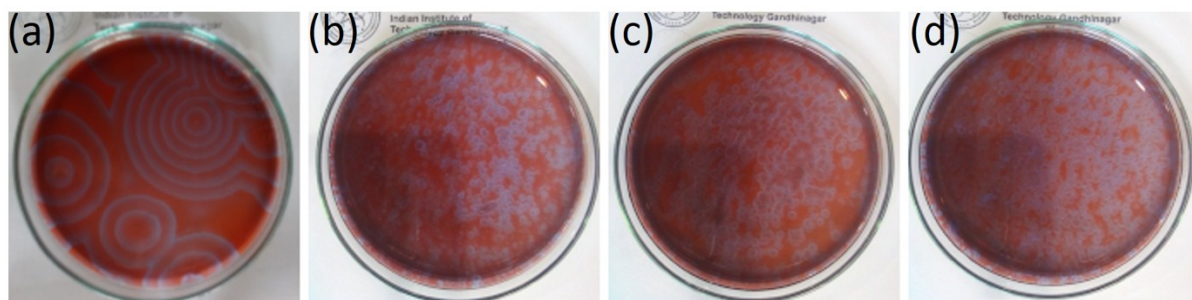


Figure S11 Waveform of BZ reaction with (a) Cerium, (b) Ru-GO, (c) Ru-rGO, and (d) Ru-graphene catalysts.

S12 Multiple runs for BZ reaction for various BZ nanocatalysts

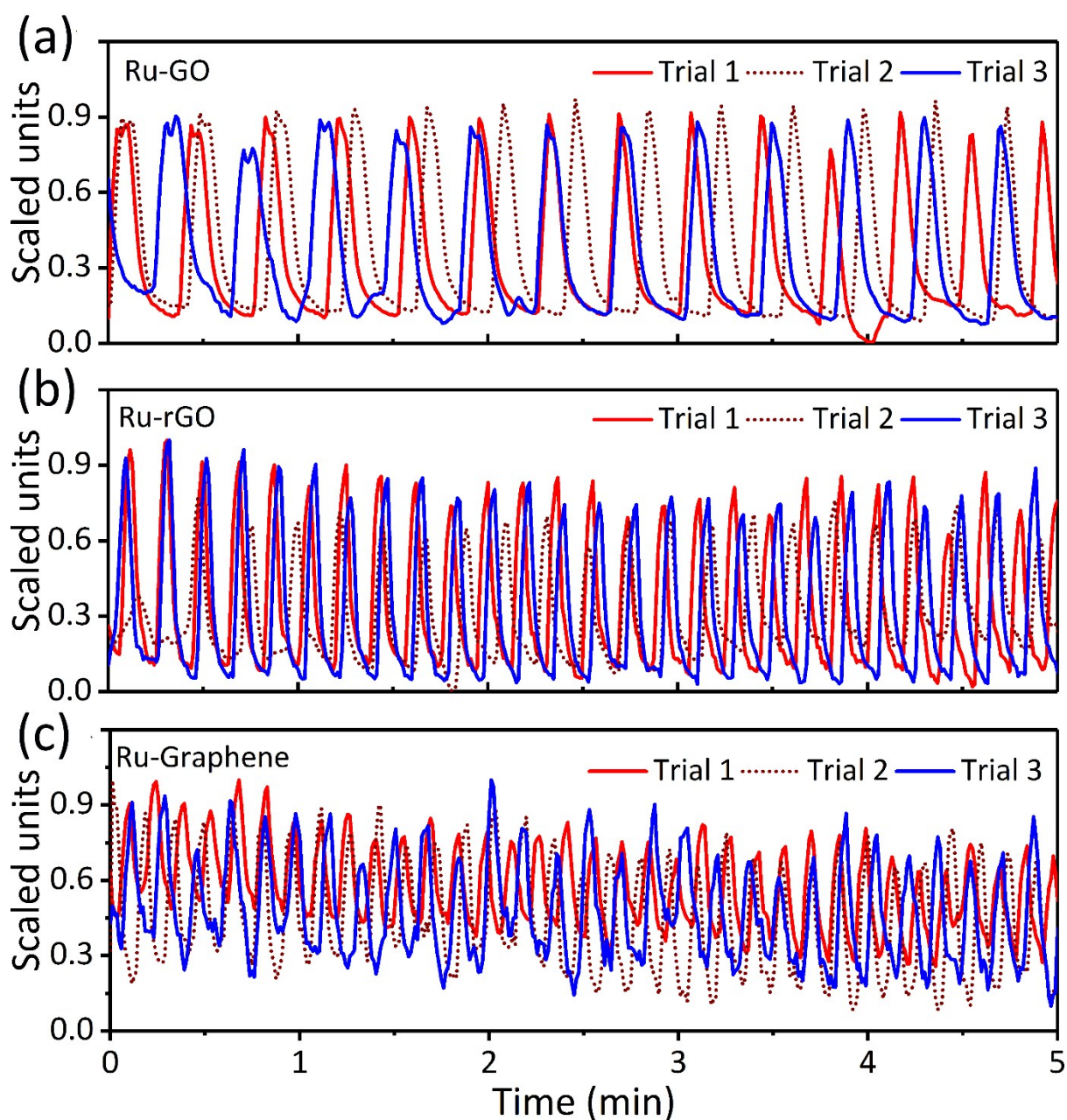


Figure S12 Variation of the intensity of BZ reaction as a function of time for Ru-GO (top panel), Ru-rGO (central panel) and Ru-graphene (bottom panel). Each panel consists of three different trials for each of the nanocomposites under identical experimental conditions. It can be observed that the frequency of chemical oscillations (number of peaks) remains constant for all the trails. The number of oscillations are highest with Ru-graphene BZ nanocatalyst.

The reproducibility in the measurement of frequency with 90% confidence interval is summarized in the Table S12. The confidence intervals are calculated using the expression, $CI = \bar{X} \pm t \frac{\sigma}{\sqrt{n}}$. Here \bar{X} is the mean, σ is standard deviation, n is number of trials, and t is the value taken from t -distribution table corresponding to the value of n and CI . In our calculations, for 90% CI over 3 number of trials, the corresponding t -value as determined from the distribution table is 2.92.

Table S12 The average frequency of BZ reaction catalyzed by various nanocatalysts with 90% confidence interval for 3 trials.

| Sample | Average frequency (mHz) | Frequency with 90% confidence interval (mHz) |
|-------------|-------------------------|--|
| Ru-GO | 43.3 | 41.7-44.3 |
| Ru-rGO | 83.3 | 70.6-95.9 |
| Ru-graphene | 116.6 | 113.9-119.5 |

References:

- 1 A. N. Zaikin and A. M. Zhabotinsky, *Nature*, 1970, **225**, 535–537.
- 2 R. Field and R. Noyes, *J. Chem. Phys.*, 1974, **60**, 1877–1884.
- 3 R. J. Field, E. Koros and R. M. Noyes, *J. Am. Chem. Soc.*, 1972, **94**, 8649–8664.
- 4 L. Gyorgyi, T. Turanyi and R. Field, *J. Phys. Chem.*, 1990, **2**, 7162–7170.
- 5 K. R. Graziani, J. L. Hudson and R. A. Schmitz, *Chem. Eng. J.*, 1976, **12**, 9–21.
- 6 G. Goncalves, P. A. A. P. Marques, C. M. Granadeiro, H. I. S. Nogueira, M. K. Singh and J. Gr, *Chem. Mater*, 2009, **21**, 4796–4802.
- 7 J. Zhang, H. Yang, G. Shen, P. Cheng, J. Zhang and S. Guo, *Chem. Commun.*, 2010, **46**, 1112–1114.
- 8 F. T. Johra, J. W. Lee and W. G. Jung, *J. Ind. Eng. Chem.*, 2014, **20**, 2883–2887.
- 9 K. Dave, K. H. Park and M. Dhayal, *RSC Adv.*, 2015, **5**, 95657–95665.
- 10 C. Du, Q. Ao, N. Cao, L. Yang, W. Luo and G. Cheng, *Int. J. Hydrogen Energy*, 2015, **40**, 6180–6187.
- 11 S. Peng, J. Liu, J. Zhang and F. Wang, *Int. J. Hydrogen Energy*, 2015, **40**, 10856–10866.
- 12 P. P. Upare, M. Lee, S.-K. Lee, J. W. Yoon, J. Bae, D. W. Hwang, U.-H. Lee, J.-S. Chang and Y. K. Hwang, *Catal. Today*, 2016, **265**, 174–183.
- 13 A. Shimamoto, K. Yamashita, H. Inoue, S. Yang, M. Iwata and N. Ike, *J. Press. Vessel Technol.*, 2013, **135**, 021501.